Cdkn2a (Arf) loss drives NF1-associated atypical neurofibroma and malignant transformation.

Steven D. Rhodes[1,2], Yongzheng He[1], Abbi Smith[1], Li Jiang[1], Qingbo Lu[1], Julie Mund[1], Xiaohong Li[1], Waylan Bessler[1], Shaomin Qian[1], William Dyer[1], George E. Sandusky[3], Andrew E. Horvai[4], Amy E. Armstrong[1,2], and D. Wade Clapp[1,*]

[1]Department of Pediatrics, Herman B. Wells Center for Pediatric Research, Indiana University School of Medicine
[2]Division of Pediatric Hematology-Oncology, Indiana University School of Medicine
[3]Department of Pathology, Indiana University School of Medicine
[4]Department of Pathology and Laboratory Medicine, University of California, San Francisco

*Correspondence should be addressed to: D. Wade Clapp, M.D. Richard L. Schreiner Professor and Chairman Department of Pediatrics, Indiana University School of Medicine Riley Hospital for Children at Indiana University Health 705 Riley Hospital Dr. Room 5900 Indianapolis, IN 46202 Phone: (317) 944-7810 Email: dclapp@iu.edu Fax: (317)-944-4471

ABSTRACT

Plexiform neurofibroma (PN) tumors are a hallmark manifestation of neurofibromatosis type 1 (NF1) that arise in the Schwann cell (SC) lineage. NF1 is a common heritable cancer predisposition syndrome caused by germline mutations in the *NF1* tumor suppressor, which encodes a GTPase activating protein called neurofibromin that negatively regulates Ras proteins. Whereas most PN are clinically indolent, a subset progress to atypical neurofibromatous neoplasms of uncertain biologic potential (ANNUBP) and/or to malignant peripheral nerve sheath tumors (MPNSTs). In small clinical series, loss of 9p21.3, which includes the *CDKN2A* locus, has been associated with the genesis of ANNUBP. Here we show that the *Cdkn2a* alternate reading frame (*Arf*) serves as a gatekeeper tumor suppressor in mice, that prevents PN progression by inducing senescence mediated growth arrest in aberrantly proliferating $Nf1^{-/-}$ PN. Conditional ablation of *Nf1* and *Arf* in the neural crest derived SC lineage allows escape from

senescence, resulting in tumors which accurately phenocopy human ANNUBP and progress to MPNST with high penetrance. This animal model will serve as a platform to study the clonal development of ANNUBP and MPNST, and to identify new therapies to treat existing tumors and to prevent disease progression.

INTRODUCTION

Neurofibromatosis type 1 (NF1) is one of the most common heritable cancer predisposition syndromes, affecting 1 in 3000 individuals in all populations throughout the world (1). Plexiform neurofibromas (PN), which are a hallmark manifestation of NF1, are benign nerve and soft tissue tumors that manifest within the nerve fascicles driven by bilallelic loss of *NF1/Nf1* in the embryonic and early neonatal Schwann lineage (SC) in human tumors and in genetically engineered murine models (2, 3). PN have a 15% lifetime incidence of transformation to highly aggressive sarcomas called malignant peripheral nerve sheath tumors (MPNST) (4), which are the leading cause of mortality in NF1 patients. Current MPNST therapies, including surgery and chemoradiotherapy, are both debilitating and largely ineffective. Understanding why some PN progress to MPNST while others remain indolent is paramount to developing effective treatment strategies for preventing disease progression and for early therapeutic intervention.

Beyond early childhood and adolescence, most PN grow slowly at a median growth rate of 3.7% per year (5). Further, some PN stop growing entirely despite persistent Ras activation. We hypothesized that PN growth arrest results from activation of a senescence program in response to chronic Ras hyperactivation. Subsequent escape from this growth arrest may ultimately drive progression of PN towards MPNST. The alternate reading frame of *CDKN2A (ARF)* encodes a

tumor suppressor gene that induces senescence-like cell cycle arrest through the stabilization of

p53 (6). Intriguingly, a number of other benign, slow growing neoplasms harboring oncogenic

RAS mutations including nevi and colonic adenomas overexpress *CDKN2A/ARF* and are

characterized by a signature of senescence prior to tumor progression (7, 8).

Longitudinal imaging studies of NF1 patients with PN have identified a subset of distinct nodular

lesions that emerge after childhood within existing PN, grow rapidly relative to the surrounding

tumor, and are FDG-PET avid (9). Biopsies often reveal atypical neurofibromatous neoplasms of

uncertain biologic potential (ANNUBP), which share some overlapping histopathological

features with MPNST and have been implicated as potential MPNST precursors (10).

Intriguingly, karyotyping and microarray analysis identified chromosome 9p21.3 deletions,

encoding the entire *CDKN2A/B* locus, as a solitary and highly recurrent genetic aberration in

human ANNUBP (94%, n=15/16) that were not present in PN (11). Further, haploinsufficient or

homozygous loss of *CDKN2A* (p16^{INK4A}) and its alternative reading frame p14^{ARF} was identified

in 60-80% of MPNSTs in two recent independent studies (12, 13).

Here we provide genetic evidence that the *Arf* tumor suppressor restrains the proliferation of *Nf1*$^{-}$
$^{/-}$ SCs. Our postulate that this phenomenon is due to the activation of a senescence program,

invoked by Ras hyperactivation, was supported by a broad signature of senescence in both

murine and human PN. Further, we show that mice harboring conditional ablation of *Nf1* and

Arf in embryonic neural crest develop tumors that are histopathologically indistinguishable from

human ANNUBP and subsequently progress to MPNST with high penetrance. Whereas germline

mouse models where *p53*(14), *p16*(15)*, or p19Arf* (16) are lost in addition to *Nf1* develop

MPNST and other sarcomas in the absence of apparent premalignant changes, the tissue lineage specific model outlined here is the first to recapitulate the malignant transformation of pre-existing PN and ANNBUP precursor lesions. Thus, this model provides a tractable platform to study the clonal development of ANNUBP and MPNSTs and evaluate novel therapeutic strategies.

RESULTS

$Nf1^{-/-}$ SCs undergo senescence induced growth arrest, driven by Ras-dependent induction of p19^{Arf} expression

To test the hypothesis that the outgrowth of $Nf1^{-/-}$ SCs is limited by senescence, we genetically ablated $Nf1$ in embryonic SC progenitors. As anticipated, this resulted in loss of neurofibromin protein expression and elevated levels of active Ras-GTP (**Figure 1A**). This hyperactivation of Ras was associated with an initial burst of increased proliferation in $Nf1^{-/-}$ SCs, which was not sustained (**Figure 1B**). Growth arrest was accompanied by robust β-galactosidase expression (**Figure 1C**), an established marker of cellular senescence. Correlating with the increase in β-galactosidase staining, the expression of the senescence associated transcripts, *Cdkn2a(Arf)* and *Cdkn2b* were upregulated 5-6 fold in $Nf1^{-/-}$ SCs relative to control wild-type (WT) SCs (**Figure 1D**). Consistent with these data, we observed robust induction of p19^{Arf}, p53, and p16^{Ink4a} protein expression in $Nf1^{-/-}$ cells by Western blot (**Figure 1E**).

Human and murine PN exhibit senescence signature

We next evaluated human and murine PN for *in vivo* evidence of a senescence signature. Human PN tumors strongly expressed senescence markers. In immunohistochemical (IHC) assays,

marked increases in the expression of p16^{INK4A}/p15^{INK4B} (**Figure 2A**) and the *CDKN2A* alternative reading frame homologue p14^{ARF} (**Figure 2B**) were observed in human PN as compared to control nerve tissues. Similar results were obtained when murine PN were assayed. *Nf1$^{flox/flox}$;PostnCre(+)* mice harboring conditional biallelic loss of *Nf1* in primitive neural crest derived progenitor SCs (the tumorigenic cell of origin for PN) driven by Cre-recombinase expressed under the control of a 3.9kb segment of the *Periostin* promoter (*PostnCre*) (17) develop tumors that are histopathologically indistinguishable from human PN. Peripheral nerve tissues and PN arising in *Nf1$^{flox/flox}$;PostnCre(+)* mice exhibited significantly increased p16^{Ink4a}/p19^{Arf} expression relative to WT controls by IHC staining (**Figure 2C, D**). Consistent with these results, p19^{Arf} expression was also significantly elevated in the trigeminal nerve of *Nf1$^{flox/flox}$;PostnCre(+)* mice, a cranial nerve that frequently develops plexiform neurofibromas in mice and humans (**Figure 2E, Supplemental Figure 1**). Immunofluorescence (IF) staining for S100 to identify neural crest derived progenitors and p16^{Ink4a}/p19^{Arf} to identify senescence revealed a high degree of coexpression. Additionally, S100-negative cells were observed as part of the tumor microenvironment (**Figure 2F**). Together with studies of cultures in primary SCs, these data indicate that murine and human PN induce known markers of cellular senescence *in vivo*.

These data led us to postulate in PN, indolence and tumor growth arrest may be controlled by p19^{Arf} tumor suppressor activity. We therefore bred *Nf1* floxed mice with mice harboring a loxP site flanking the first coding exon (exon-1β) of the *Arf* gene, facilitating Cre-mediated excision of *Arf* but leaving the linked *Ink4a* (*Cdkn2a*) gene intact (18). Embryonic dorsal root ganglion (DRG)/nerve root neurosphere cells (DNSCs) were isolated from the resulting *Nf1$^{flox/flox}$*,

Nf1^{flox/flox};Arf^{flox/+} and *Nf1^{flox/flox;}Arf^{flox/flox}* genotypes and infected with Cre recombinase expressing adenovirus or empty vector control. These cells contain the neural crest derived tumorigenic cell of origin for PNs (2). Efficient Cre-mediated excision of floxed *Nf1* and *Arf* alleles and corresponding loss of protein expression were confirmed by PCR (**Supplemental Figure 2A**) and western blot, respectively (**Supplemental Figure 2B**). *Nf1-Arf* double knockout (DKO, *Nf1^{-/-}; Arf^{-/-}*) DNSCs demonstrated increased proliferation compared to WT and *Nf1^{-/-}* DNSCs in a gene dosage dependent fashion (**Figure 3A**). Proliferation was confirmed via increased cell-cycle entry into S-phase (**Figure 3B**) of the *Nf1^{-/-};Arf^{-/-}* DNSCs. Unlike *Nf1^{-/-}* DNSCS which exhibited increased senescence, *Nf1^{-/-};Arf^{+/-}* and *Nf1^{-/-};Arf^{-/-}* DNSCs cultures were devoid of senescent cells (**Figure 3C, D**). However, the percentage of S-phase cells was significantly higher in homozygous *Arf*-mutant DNSCs (**Figure 3B**). These data indicate that *Arf* inactivation increases the proliferation of *Nf1* mutant DNSCs in a dose-dependent manner with loss of a single *Arf* allele overcoming the cellular program invoked by loss of *Nf1*.

Arf Nf1^{-/-} SC progenitors phenocopy human ANNUBP

To examine whether *Arf* loss could directly mediate progression from PN to ANNUBP we conditionally ablated *Arf* in the murine model of *Nf1* PN. Following Cre mediated recombination and incubation of the mutant mice, microdissection of the lumbosacral nerve plexus revealed a generalized thickening of the proximal spinal nerve roots as well as multiple discrete tumors arising adjacent to the DRG of *Nf1^{flox/flox}*, *Nf1^{flox/flox};Arf^{flox/+}* and *Nf1^{flox/flox};Arf^{flox/flox};PostnCre(+)* mutant mice (**Figure 4A, B**). *Arf^{flox/flox};PostnCre(+)* mice revealed normal nerve root morphology and architecture (**Supplemental Figure 3**). Western blot of *Nf1/Arf* intercrossed mice confirmed loss of p19^{Arf} expression (**Figure 4C**).

Histopathological evaluation confirmed the presence of PNs along multiple proximal spinal nerve roots in $Nf1^{flox/flox}$,$Nf1^{flox/flox}$;$Arf^{flox/+}$ and $Nf1^{flox/flox}$;$Arf^{flox/flox}$;$PostnCre(+)$ mutant mice with disrupted nerve architecture, wavy S100+ SCs, increased collagen deposition and mast cell infiltration (**Table 1 and Supplemental Figure 4**). Interestingly, $Nf1^{flox/flox}$;$Arf^{flox/+}$ and $Nf1^{flox/flox}$;$Arf^{flox/flox}$;$PostnCre(+)$ mice also showed outgrowths from peripheral nerves with unique histopathological changes not seen in the $Nf1^{flox/flox}$;$PostnCre(+)$ mice beginning at approximately 4 months of life. These lesions met the diagnostic criteria for human ANNUBP based on the presence of increased cellularity, cytological atypia (enlarged, hyperchromatic nuclei), a fascicular growth pattern and loss of the lattice like CD34+ fibroblastic network seen in PN (**Table 1, Figure 5, Supplemental Figure 4**). Importantly, these lesions also lacked mitotic features required for the diagnosis of low grade MPNST. Cervicothoracic spines and associated nerve roots were embedded, sectioned and examined systematically at each spinal level to identify the presence of tumors meeting diagnostic criteria for PN and ANNUBP (**Figure 6A**). The proportion of PN and ANNUBP was similar between $Nf1^{flox/flox}$;$Arf^{flox/+}$ and $Nf1^{flox/flox}$;$Arf^{flox/flox}$;$PostnCre(+)$ mice (**Figure 6B**) at approximately 6 months of age. Further, while the overall mean proximal nerve root volume was similar amongst the $Nf1^{flox/flox}$ and $Nf1$-Arf intercrossed mice, the size of ANNUBP was significantly larger than PN in the same mouse, regardless of genotype (**Figure 6C**).

Spontaneous progression of ANNUBP to MPNST

A distinguishing feature of $Nf1^{flox/flox}$;$Arf^{flox/flox}$;$PostnCre(+)$ mice was the early development of infiltrating and rapidly growing tumors arising from existing PN and ANNUBP lesions (**Figure 7A, B**) which met diagnostic criteria for MPNST (**Table 1 and Supplemental Figure 4**).

Nf1$^{flox/flox}$*;Arf*$^{flox/flox}$*;PostnCre(+)* mice die of MPNST with 100% penetrance (n =16/16) and a mean survival time of 4.8 months. *Arf* heterozyous *Nf1*$^{flox/flox}$*;Arf*$^{flox/+}$*;PostnCre(+)* mice exhibit haploinsufficiency with delayed MPNST onset, and a mean survival time of 8.7 months (**Figure 7C**). A subset of *Nf1*$^{flox/flox}$*;PostnCre(+)* mice also die from PN nerve compression of vital structures. Mice containing a disruption of the *Arf* allele in Schwann cells did not form tumors (**Supplemental Figure 3**). Collectively, the present results demonstrate causality of sequential *Nf1* and *Arf* loss in the progression of PN to ANNUBP and MPNST. In addition, immunofluorescence and immunohistochemical stains against p16^{Ink4a}/p19^{Arf} and pRb confirm loss of the senescence signature *in vivo* with progression of PN to ANNUBP and MPNST (**Supplemental Figure 5**).

DISCUSSION

Mammalian cells have developed intricate mechanisms to prevent pathological stimuli resulting in cells undergoing tumorigenesis and transformation. When constitutively active stimuli are present, such as chronic oncogenic signaling, tumor suppressor networks are engaged that antagonized aberrant proliferation by mechanisms that include the induction of cellular senescence. The expression of oncogenic Ras induces senescence-like growth arrest in primary cells and is regarded a major mechanism to prevent the proliferation of incipient cancer cells (19). Colonic serated adenomas initiated oncogenic Kras^{G12D}, overexpress p16^{INK4A} and undergo senescence (8). Their progression to malignant adenocarcinomas is linked to *Ink4/Arf* ablation. Similarly, benign melanocytic human nevi, harboring *BRAF*^{V600E} mutations, have been shown to over-express p16^{INK4A}, and acquire *CDKN2A* mutations upon progression to malignant melanoma (20). Previously, Courtois-Cox et al. reported that loss of *NF1* induced a senescence

in human fibroblasts through up-regulation of p16 (21). Here we show that loss of *Nf1* leads to hyperactive Ras and increased senescence in primary Schwann cells consistent with these other disease models.

Human genetic data from small case series in neurofibromas have led to speculation whether haploinsufficient or nullizygous loss of *CDKN2A/B* is necessary and/or sufficient to promote ANNUBP and subsequent progression to MPNST. One series used microarray to implicate chromosome 9p21.3 band deletions as the predominating genetic driver of ANNUBP (11). A second study, consisting of PN and a single ANNUBP suggested that heterozygous loss of *CDKN2A* was sufficient to generate cytologic atypia, but nullizygous loss was required for the formation of ANNUBP (22). A confounding feature of both studies was the presence of additional gene mutations including known tumor suppressors. The power of genetically engineered mouse models allowed us to focus specifically on *Arf* in the context of *Nf1* mediated PN formation. Our experimental findings indicate that inactivating a single allele of *Arf* in *Nf1* deficient SCs is sufficient to promote the genesis of ANNUBP and MPNST. These findings suggest that loss of heterozygosity (LOH) of *Arf* is not required for the development of ANNUBP or malignant transformation. Additional analysis will be required to better understand the detailed dynamics of the initiating events.

Developing effective strategies to treat orphan cancers with limited numbers of patients remains a clinical challenge. Genetically engineered mouse (GEM) models have demonstrated their utility to provide mechanistic insights into the biology of these tumors, thereby serving as a catalyst for drug discovery. In particular, genetic and pharmacologic studies in NF1-associated

GEM models have predicted patient responses and provided insights into future trials with high fidelity (23-26). The studies outlined here thus provide a potential opportunity for treatment and prevention of ANNUBP and MPNSTs. It remains to be determined whether the majority of ANNUBP will respond to MEK and other single agent RTK inhibitors that have shown some efficacy in treating PN (27, 28). Further, the observation that human ANNUBP and many MPNST are *Ink4/Arf* deficient but p53 competent, provides a unique window of therapeutic opportunity for drugs such as MDM2 and/or CDK4/6 inhibitors as potential avenues of treatment.

MATERIALS AND METHODS

Experimental animals and genotyping

The genetically engineered *Nf1* floxed, *Arf* floxed and *PostnCre* mice were utilized for *in vivo* studies, with genotypes confirmed by polymerase chain reaction (PCR) as described. The WT,*Nf1* floxed, and recombination bands were detected using the following primers: P1: 5'-AATGTGAAATTGGTGTCGA GTAAGGTAACCAC 3', P2: 5'-TTAAGAGCATCTGCTGCTCTTAGAGGGAA 3', P3: 5'- TCAG ACTGATTGTTGTACCTGATGGTTGTACC 3'. The *Arf* floxed band was detected using forward primer: 5'- ACTGCAGCCAGACCACTAGG 3' and reverse primer: 5'-AGCTCGGAGATTG AGAAAGC 3'. *PostnCre* was detected using forward primer: 5'-ATGTTTAGCTGGCCCAAATG-3' and reverse primer: 5'-CGACCACTACCAGCAGAACA-3'. Animal care and experiments were conducted according to the guidelines established by the Indiana University Animal Care and Use Committee (IACUC).

Nerve tree microdissection and measurement of tumor volume

Immediately postmortem, fresh blood and select tissues were harvested and mice were perfused and fixed in 10% neutral buffered formalin. The bodies were decalcified in a 50:50 solution of 10% formic acid and 10% neutral buffered formalin solution. The proximal spinal nerve roots from the lumbosacral spine were dissected microscopically. The volume of proximal peripheral nerves was determined using calipers to measure the length and width of dissected tumors (or equivalent region in absence of tumor) in maximal dimension. Volume was then approximated using the formula for the volume of a spheroid $= 0.52 \times (\text{width})^2 \times \text{length}$.

Histopathology

Cervical and thoracic spines with associated DRG and proximal spinal nerve roots were excised from euthanized animals, fixed with 10% formalin, decalcified, dehydrated with graded alcohols, cleared with xylenes, infiltrated with molten paraffin, and embedded in paraffin blocks. Five micron thick sections were cut on a Leica rotary microtome, and stained with hematoxylin and eosin (H&E). Mice were also carefully examined for evidence of gross tumors which were dissected and excised, formalin fixed, processed, and paraffin-embedded for histopathological analysis. The liver and lungs were also harvested to evaluate for evidence of metastatic disease. Plexiform neurofibroma (PN), atypical neurofibromas of uncertain biological potential (ANNUBP) and malignant peripheral nerve sheath tumors (MPNST) were identified according to criteria adopted from a recent consensus overview by Miettinen et al. (10) and are outlined in **Table 1**.

Immunohistochemistry

Paraffin sections were deparaffinized, hydrated and transferred to 0.1 M citrate buffer (pH 6.0) for antigen retrieval. Slides were pressure cooked for 3 minutes in citrate buffer, cooled for 1 hour, then rinsed in distilled water. Sections were quenched with 3% hydrogen peroxide for 10 minutes, rinsed in distilled water, and blocked in 5% normal goat serum in TBST (TBS buffer + 0.1% tween 20). Sections were incubated overnight at 4°C in primary antibody diluted in blocking buffer; S100 (z0311, 1:400 dilution, Dako), CD34 (ab81289, 1:2500 dilution, Abcam), H3K27me (CST9733, 1:200 dilution, Cell Signaling Technology), p16^{Ink4a}/p19^{Arf} (ab54210, 1:500 dilution, Abcam), p15^{INK4B}/p16^{INK4A} (sc377412, 1:250 dilution, Santa Cruz Biotechnology) and p14^{ARF} (CST2407, 1:50 dilution, Cell Signaling Technology). Sections were then incubated in appropriate biotinylated secondary antibodies for 1 hour at room temperature; goat anti-rabbit (B8895, 1:800, Sigma). Vectastain Elite ABC reagent was applied for 30 minutes at room temperature. Color development with Vectastain DAB was observed under the microscope and the reaction was terminated by rinsing in distilled water. Sections were counterstained with modified Mayer's Hematoxylin (Vector), dehydrated, cleared and coverslipped. When anti-mouse primary antibody was used, Rodent Block M (BioCare Medical Mouse-on-Mouse HRP Polymer kit, MM510) was applied for 30 minutes at room temperature instead of blocking buffer for 1 hour. Additionally, Mouse-on-mouse HRP polymer was applied for 15 minutes at room temperature instead of the secondary antibody and ABC reagent. Statistical comparisons between control and tumor samples were conducted using Student's t test. Whole slide images were acquired on Aperio ScanScope CS and QImaging Retiga 2000R camera on a Nikon Eclipse 80i microscope.

Immunofluorescence

Paraffin sections were deparaffinized, hydrated and transferred to 0.1 M citrate buffer (pH 6.0) for antigen retrieval. Slides were pressure cooked for 3 minutes in citrate buffer, cooled for 1 hour, then rinsed in distilled water. Sections were quenched with 3% hydrogen peroxide for 10 minutes, rinsed in distilled water, and blocked in Rodent Block M (BioCare Medical Mouse-on-Mouse HRP Polymer kit, MM510) for 30 min. Sections were incubated at 4°C overnight in primary antibodies diluted in blocking buffer (5% normal goat serum in TBST); S100 (z0311, 1:400 dilution, Dako) and p16^{Ink4a}/p19^{Arf} (ab54210, 1:400, Abcam). Sections were then incubated in appropriate fluorophore-conjugated secondary antibodies for 1 hour at room temperature; goat anti-rabbit 488 (A11034; 1:1000, Invitrogen), goat anti-mouse 568 (A11031, 1:1000, Invitrogen). Slides were then rinsed and stained with Hoechst 33342 (1:5000, Molecular Probes) for 5 minutes at room temperature. Autofluorescence was quenched with Vector TrueVIEW. Slides were coverslipped and imaged on the QImaging Retiga 2000R camera on a Nikon Eclipse 80i microscope, using an X-Cite 120 fluorescence lamp. Merged images were processed using NIH Image J software.

DNSC isolation and culture

Mouse embryos were removed from pregnant female mice at E13.5 following euthanasia. The dorsal root ganglia (DRG) and spinal nerve roots were microdissected under a stereomicroscope. DRG and/or nerve root neurosphere culture was performed in serum-free DMEM/F12 media containing penicillin/streptomycin (0.1%); fungizone (40 mg/mL); B27 (without vitamin A), epidermal growth factor (20 ng/mL), and basic fibroblast growth factor (40 ng/mL; Sigma). The sphere cells were fed every 3–4 days and passaged upon reaching confluence. Retaining one-third of the conditioned medium with fresh medium changes.

Schwann cell differentiation from DNSCs

25,000 DNSCs were seeded on fibronectin coated 12 well plates and cultured in DMEM/F12 media supplemented with 10% FBS and nerve growth factor (NGF) 200 ng/mL for 6 days.

Proliferation assays

DNSCs were seeded on fibronectin coated 12 well plates at a density of 50,000 cells per well and cultured in serum-free DMEM/F12 media containing penicillin/streptomycin (0.1%); fungizone (40 mg/mL); B27 (without vitamin A), epidermal growth factor (20 ng/mL), and basic fibroblast growth factor (40 ng/mL; Sigma). Viable cells as determined by trypan blue dye exclusion, were counted manually on a glass hemocytometer.

Quantitative RT-PCR

mRNAs were isolated from primary Schwann cells cultured from WTand $Nf1^{flox/flox}$;PostnCre mice using PureLink RNA Micro Kit (Cat#15596026, Thermofisher). mRNA was reverse-transcribed to cDNA using High-Capacity cDNA Reverse Transcription Kit with RNase Inhibitor Cat#4374966, Thermofisher). Primers were obtained from Invitrogen for quantitative RT-PCR (qRT-PCR) using SYBER-green(Cat#4385612, Thermofisher). The sequence of forward and reverse primers utilized for qRT-PCR was as follows: *Cdkn2a* (variant 1(*Arf*)) forward primer 5′- CATGTTGTTGAGGCTAGAGAGG-3′; *Cdkn2a* reverse primer: 5′-TGAGCAGAAGAGCTGCTACG-3′; *Cdkn2b* forward primer: 5′-CCCTGCCACCCTTACCAGA -3′; *Cdkn2b* reverse primer: 5'-GCAGATACCTCGCAATGTCAC- 3'. *Gapdh* forward primer 5'-TGATGACATCAAGAAGGTGGTGAAG-3'; *Gapdh* reverse primer 5'-

TCCTTGGAGGCCATGTAGGCCAT-3'. Triplicate reactions were performed on an Applied

Biosystems 7500 Real-Time PCR instrument. Relative gene expression was normalized to

endogenous *Gapdh*. The fold change in *Cdkn2a* and *Cdkn2b* in *Nf1*^{-/-} Schwann cells relative to

WT was determined using the ΔΔCT method.

Senescence

Cellular senescence was assessed by β-galatosidase utilizing a Senescence Cells Histochemial

Staining Kit (CS0030, Sigma). Briefly, growth medium was aspirated from adherent cells in

culture. Cells were washed twice and fixed for 8 minutes at room temperature. Cells were then

incubated with β-galactosidase (β-gal) staining mixture at 37°C without CO_2 for 4 hours or until

blue staining was apparent. β-gal stained cells and total cells were counted on photomicrographs

acquired at high power. The percentage of senescence cells expressing β-gal was determined.

Ras activity assays

A non-radioative Ras Activation Assay Kit (#17-218, Millipore) was used to detect and GTP-

bound Ras in DNSC lysates. DNSCs were cultured to approximately 90% confluence in 10-cm

dishes. Upon removal of culture media, cells were rinsed 2x with ice cold PBS, followed by the

addition of ice cold 500 µL MLB containing 10% glycerol, prepared according to the

manufacturers recommendation. A cell scraper was used to detach cells from plates and lysates

were transferred to microfuge tubes on ice, followed by sonication for 5 seconds twice at a

frequency of 12 KHz. Insoluble cellular debris was pelleted by centrifugation at 14,000xg for 5

minutes at 4°C. The extract (supernatant) was removed, flash frozen, and stored at -80°C for

future use. Pull down of Ras-GTP was performed using 10 µg of Ras assay reagent (Raf-1 RBD,

agarose), which was added to each cell extract and incubated for 45 minutes with gentle agitation at 4°C. Agarose beads were pelleted by brief centrifugation (10 sec, 14,000xg, 4°C). The supernatant was removed and discarded. Beads were washed 3x with 500 µL MLB, followed by resuspension in 40 µL of 2x Laemmli reducing buffer with 2 µL of 1M dithioteritol and boiled for 5 minutes to release GTP-bound Ras from the beads. Ras-GTP was detected by western blot, incubating with anti-Ras, clone RAS10 (# 05-516, Millipore) diluted in freshly prepared PBST-MLK overnight with agitation and goat anti-mouse-HRP conjugate (# 12-349, Millipore) as directed.

Western blot

Isolated proteins were fractionated using NuPAGE 4-12% Bis-Tris Gels (Invitrogen Cat#NP0322BOX) and electro-transferred to PVDF membranes. Immunoblots were carried out using antibodies specific to p19^{Arf} (Cat#05-929, EMD), p16^{Ink4a}/p15^{Ink4b} (Cat#377412, Santa Cruz), p53 (Cat#CST-2524, Cell Signaling Technology), neurofibromin (#SC-67, Santa Cruz), and Gapdh (#CST-5174, Cell Signaling Technology). After incubation with appropriate HRP conjugated secondary antibodies (Anti-rabbit (#NA934V,GE Healthcare), Anti-Rat(#AP-136P, EMD), signals were detected using ECL chemoluminescence substrate (ECL Prime, GE Healthcare).

Statistical analysis

Statistical analyses were performed with GraphPad Prism 7.0 software (GraphPad, La Jolla, CA). Analysis of variance (ANOVA) and Student's t-tests with post-hoc correction for multiple comparisons were used to evaluate for statistically significant differences between samples as

described in detail within the figure legends. Statistical analysis of Kaplan Meier survival curves was performed in SAS software using a logrank test with Bonferroni post-hoc adjustment for multiple comparisons.

CONFLICT OF INTEREST STATEMENT

The authors have no conflicts of interest to disclose.

REFERENCES

1 Carey, J.C., Baty, B.J., Johnson, J.P., Morrison, T., Skolnick, M. and Kivlin, J. (1986) The genetic aspects of neurofibromatosis. *Annals of the New York Academy of Sciences*, **486**, 45-56.

2 Chen, Z., Liu, C., Patel, A.J., Liao, C.P., Wang, Y. and Le, L.Q. (2014) Cells of origin in the embryonic nerve roots for NF1-associated plexiform neurofibroma. *Cancer Cell*, **26**, 695-706.

3 Zhu, Y., Ghosh, P., Charnay, P., Burns, D.K. and Parada, L.F. (2002) Neurofibromas in NF1: Schwann cell origin and role of tumor environment. *Science*, **296**, 920-922.

4	Evans, D.G., Baser, M.E., McGaughran, J., Sharif, S., Howard, E. and Moran, A. (2002) Malignant peripheral nerve sheath tumours in neurofibromatosis 1. *J Med Genet*, **39**, 311-314.

5	Nguyen, R., Dombi, E., Widemann, B.C., Solomon, J., Fuensterer, C., Kluwe, L., Friedman, J.M. and Mautner, V.F. (2012) Growth dynamics of plexiform neurofibromas: a retrospective cohort study of 201 patients with neurofibromatosis 1. *Orphanet J Rare Dis*, **7**, 75.

6	Honda, R. and Yasuda, H. (1999) Association of p19(ARF) with Mdm2 inhibits ubiquitin ligase activity of Mdm2 for tumor suppressor p53. *EMBO J*, **18**, 22-27.

7	Romagosa, C., Simonetti, S., Lopez-Vicente, L., Mazo, A., Lleonart, M.E., Castellvi, J. and Ramon y Cajal, S. (2011) p16(Ink4a) overexpression in cancer: a tumor suppressor gene associated with senescence and high-grade tumors. *Oncogene*, **30**, 2087-2097.

8	Bennecke, M., Kriegl, L., Bajbouj, M., Retzlaff, K., Robine, S., Jung, A., Arkan, M.C., Kirchner, T. and Greten, F.R. (2010) Ink4a/Arf and oncogene-induced senescence prevent tumor progression during alternative colorectal tumorigenesis. *Cancer Cell*, **18**, 135-146.

9	Higham, C.S., Dombi, E., Rogiers, A., Bhaumik, S., Pans, S., Connor, S.E.J., Miettinen, M., Sciot, R., Tirabosco, R., Brems, H. *et al.* (2018) The characteristics of 76 atypical neurofibromas as precursors to neurofibromatosis 1 associated malignant peripheral nerve sheath tumors. *Neuro Oncol*, **20**, 818-825.

10	Miettinen, M.M., Antonescu, C.R., Fletcher, C.D.M., Kim, A., Lazar, A.J., Quezado, M.M., Reilly, K.M., Stemmer-Rachamimov, A., Stewart, D.R., Viskochil, D. *et al.* (2017) Histopathologic evaluation of atypical neurofibromatous tumors and their transformation into malignant peripheral nerve sheath tumor in patients with neurofibromatosis 1-a consensus overview. *Hum Pathol*, **67**, 1-10.

11	Beert, E., Brems, H., Daniels, B., De Wever, I., Van Calenbergh, F., Schoenaers, J., Debiec-Rychter, M., Gevaert, O., De Raedt, T., Van Den Bruel, A. *et al.* (2011) Atypical neurofibromas in neurofibromatosis type 1 are premalignant tumors. *Genes Chromosomes Cancer*, **50**, 1021-1032.

12	Brohl, A.S., Kahen, E., Yoder, S.J., Teer, J.K. and Reed, D.R. (2017) The genomic landscape of malignant peripheral nerve sheath tumors: diverse drivers of Ras pathway activation. *Sci Rep*, **7**, 14992.

13   Lee, W., Teckie, S., Wiesner, T., Ran, L., Prieto Granada, C.N., Lin, M., Zhu, S., Cao, Z., Liang, Y., Sboner, A. *et al.* (2014) PRC2 is recurrently inactivated through EED or SUZ12 loss in malignant peripheral nerve sheath tumors. *Nat Genet*, **46**, 1227-1232.

14   Vogel, K.S., Klesse, L.J., Velasco-Miguel, S., Meyers, K., Rushing, E.J. and Parada, L.F. (1999) Mouse tumor model for neurofibromatosis type 1. *Science*, **286**, 2176-2179.

15   Buchstaller, J., McKeever, P.E. and Morrison, S.J. (2012) Tumorigenic cells are common in mouse MPNSTs but their frequency depends upon tumor genotype and assay conditions. *Cancer Cell*, **21**, 240-252.

16   King, D., Yang, G., Thompson, M.A. and Hiebert, S.W. (2002) Loss of neurofibromatosis-1 and p19(ARF) cooperate to induce a multiple tumor phenotype. *Oncogene*, **21**, 4978-4982.

17   Lindsley, A., Snider, P., Zhou, H., Rogers, R., Wang, J., Olaopa, M., Kruzynska-Frejtag, A., Koushik, S.V., Lilly, B., Burch, J.B. *et al.* (2007) Identification and characterization of a novel Schwann and outflow tract endocardial cushion lineage-restricted periostin enhancer. *Dev Biol*, **307**, 340-355.

18   Gromley, A., Churchman, M.L., Zindy, F. and Sherr, C.J. (2009) Transient expression of the Arf tumor suppressor during male germ cell and eye development in Arf-Cre reporter mice. *Proc Natl Acad Sci U S A*, **106**, 6285-6290.

19   Serrano, M., Lin, A.W., McCurrach, M.E., Beach, D. and Lowe, S.W. (1997) Oncogenic ras provokes premature cell senescence associated with accumulation of p53 and p16INK4a. *Cell*, **88**, 593-602.

20   Damsky, W.E. and Bosenberg, M. (2017) Melanocytic nevi and melanoma: unraveling a complex relationship. *Oncogene*, **36**, 5771-5792.

21   Courtois-Cox, S., Genther Williams, S.M., Reczek, E.E., Johnson, B.W., McGillicuddy, L.T., Johannessen, C.M., Hollstein, P.E., MacCollin, M. and Cichowski, K. (2006) A negative feedback signaling network underlies oncogene-induced senescence. *Cancer Cell*, **10**, 459-472.

22   Carrio, M., Gel, B., Terribas, E., Zucchiatti, A.C., Moline, T., Rosas, I., Teule, A., Ramon, Y.C.S., Lopez-Gutierrez, J.C., Blanco, I. *et al.* (2018) Analysis of intratumor heterogeneity in

Neurofibromatosis type 1 plexiform neurofibromas and neurofibromas with atypical features: Correlating histological and genomic findings. *Hum Mutat*, **39**, 1112-1125.

23   Staser, K., Park, S.J., Rhodes, S.D., Zeng, Y., He, Y.Z., Shew, M.A., Gehlhausen, J.R., Cerabona, D., Menon, K., Chen, S. *et al.* (2013) Normal hematopoiesis and neurofibromin-deficient myeloproliferative disease require Erk. *J Clin Invest*, **123**, 329-334.

24   Chang, T., Krisman, K., Theobald, E.H., Xu, J., Akutagawa, J., Lauchle, J.O., Kogan, S., Braun, B.S. and Shannon, K. (2013) Sustained MEK inhibition abrogates myeloproliferative disease in Nf1 mutant mice. *J Clin Invest*, **123**, 335-339.

25   Jessen, W.J., Miller, S.J., Jousma, E., Wu, J., Rizvi, T.A., Brundage, M.E., Eaves, D., Widemann, B., Kim, M.O., Dombi, E. *et al.* (2013) MEK inhibition exhibits efficacy in human and mouse neurofibromatosis tumors. *J Clin Invest*, **123**, 340-347.

26   Yang, F.C., Ingram, D.A., Chen, S., Zhu, Y., Yuan, J., Li, X., Yang, X., Knowles, S., Horn, W., Li, Y. *et al.* (2008) Nf1-dependent tumors require a microenvironment containing Nf1+/-- and c-kit-dependent bone marrow. *Cell*, **135**, 437-448.

27   Dombi, E., Baldwin, A., Marcus, L.J., Fisher, M.J., Weiss, B., Kim, A., Whitcomb, P., Martin, S., Aschbacher-Smith, L.E., Rizvi, T.A. *et al.* (2016) Activity of Selumetinib in Neurofibromatosis Type 1-Related Plexiform Neurofibromas. *N Engl J Med*, **375**, 2550-2560.

28   Robertson, K.A., Nalepa, G., Yang, F.C., Bowers, D.C., Ho, C.Y., Hutchins, G.D., Croop, J.M., Vik, T.A., Denne, S.C., Parada, L.F. *et al.* (2012) Imatinib mesylate for plexiform neurofibromas in patients with neurofibromatosis type 1: a phase 2 trial. *Lancet Oncol*, **13**, 1218-1224.

Figure 1. Loss of neurofibromin drives Schwann cell senescence

A. Ras-GTP activity, neurofibromin and Gapdh (loading control) were detected in WT and $Nf1^{-/-}$ SC progenitors by western blot.

B. Proliferation of WT and $Nf1^{-/-}$ SCs was assessed by manual cell counting. $n=3$ biological replicates per genotype at each timepoint. ***$p<0.001$ WT vs $Nf1^{-/-}$ by two-way ANOVA.

C. Representative photomicrographs of β-galactosidase stained WT and $Nf1^{-/-}$ primary SCs. The percentage of β-galactosidase positive staining cells was quantified. $n=3$ biological replicates per genotype. ****$p<0.0001$ WT vs $Nf1^{-/-}$ by Student's t-test.

D. Expression of senescence associated transcripts,*Cdkn2a(Arf)* and *Cdkn2b* in WT and $Nf1^{-/-}$ SCs. N=3 biological replicates per genotype. *$p<0.05$ WT vs $Nf1^{-/-}$ by Student's t-test.

E. Western blot of p19^{Arf}, p53, p16^{Ink4a}, p15^{Ink4b}, and Gapdh (loading control) in WT and $Nf1^{-/-}$ SCs.

A

WT   *Nf1*⁻′⁻

Ras-GTP

Neurofibromin

Gapdh

B

WT
Nf1⁻′⁻

Cell number (x10⁴)

Days

***

C

WT

Nf1⁻′⁻

% SA- β-gal

WT   *Nf1*⁻′⁻

****

D

WT
Nf1⁻′⁻

Fold change mRNA exp.

Cdkn2a (Arf)   *Cdkn2b*

E

WT   *Nf1*⁻′⁻

p19^Arf

p53

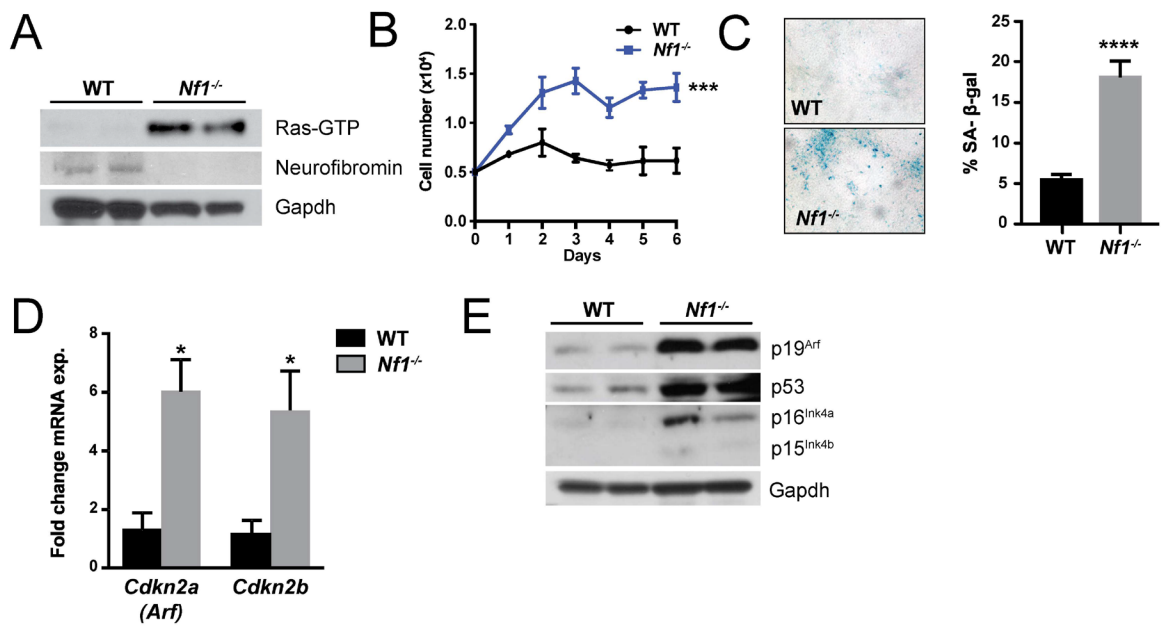p16^Ink4a

p15^Ink4b

Gapdh

Figure 1

Figure 2. Murine and human plexiform neurofibroma exhibit a senescence signature

A. Immunohistochemical (IHC) staining for $p16^{INK4A}/p15^{INK4B}$ was performed on human plexiform neurofibroma and healthy control nerve tissues. The percentage of $p16^{INK4}$ positive staining cells was quantified. $n=8$ biological replicates for plexiform neurofibroma and $n=7$ biological replicates for control nerve tissue. ** $p<0.01$ plexiform neurofibroma vs normal nerve control by Student's t-test.

B. IHC for $p14^{ARF}$ in human plexiform neurofibroma and healthy control nerve tissues. The percentage of $p14^{ARF}$ positive staining cells was quantified. $n=8$ biological replicates for plexiform neurofibroma and $n=4$ biological replicates for control nerve tissue. ** $p<0.01$ plexiform neurofibroma vs normal nerve control by Student's t-test.

C. IHC staining of $p16^{Ink4a}/p19^{Arf}$ expression in peripheral nerve tissue from WT and plexiform neurofibroma bearing $Nf1^{flox/flox};PostnCre(+)$ mice.

D. The percentage of $p16^{Ink4a}/p19^{Arf}$-positive staining cells was quantified. $n=3$ biological replicates per group. * $p<0.05$ for WT vs $Nf1^{flox/flox};PostnCre$ nerve and tumor tissue. No-statistically significant difference (ns) comparing $Nf1^{flox/flox};PostnCre$ nerve and tumor bearing tissue.

E. Western blot of $p19^{Arf}$ and Gapdh in the trigeminal nerve tissues of WT and $Nf1^{flox/flox};PostnCre(+)$ mice. Expression was normalized to Gapdh and quantified in relative densitometry units (RDU). ** $p<0.01$ WT vs $Nf1^{flox/flox};PostnCre(+)$ by one-way ANOVA followed by Tukey's multiple comparisons test. $n=5$ biological replicates per genotype as shown on expanded panel in Supplemental Figure 1.

F. Immunofluorescence with anti-S100 (GFP), anti-p16^{Ink4a}/p19^{Arf} (RFP), and nuclear

(DAPI) markers. Representative merged photomicrographs are shown at 20x
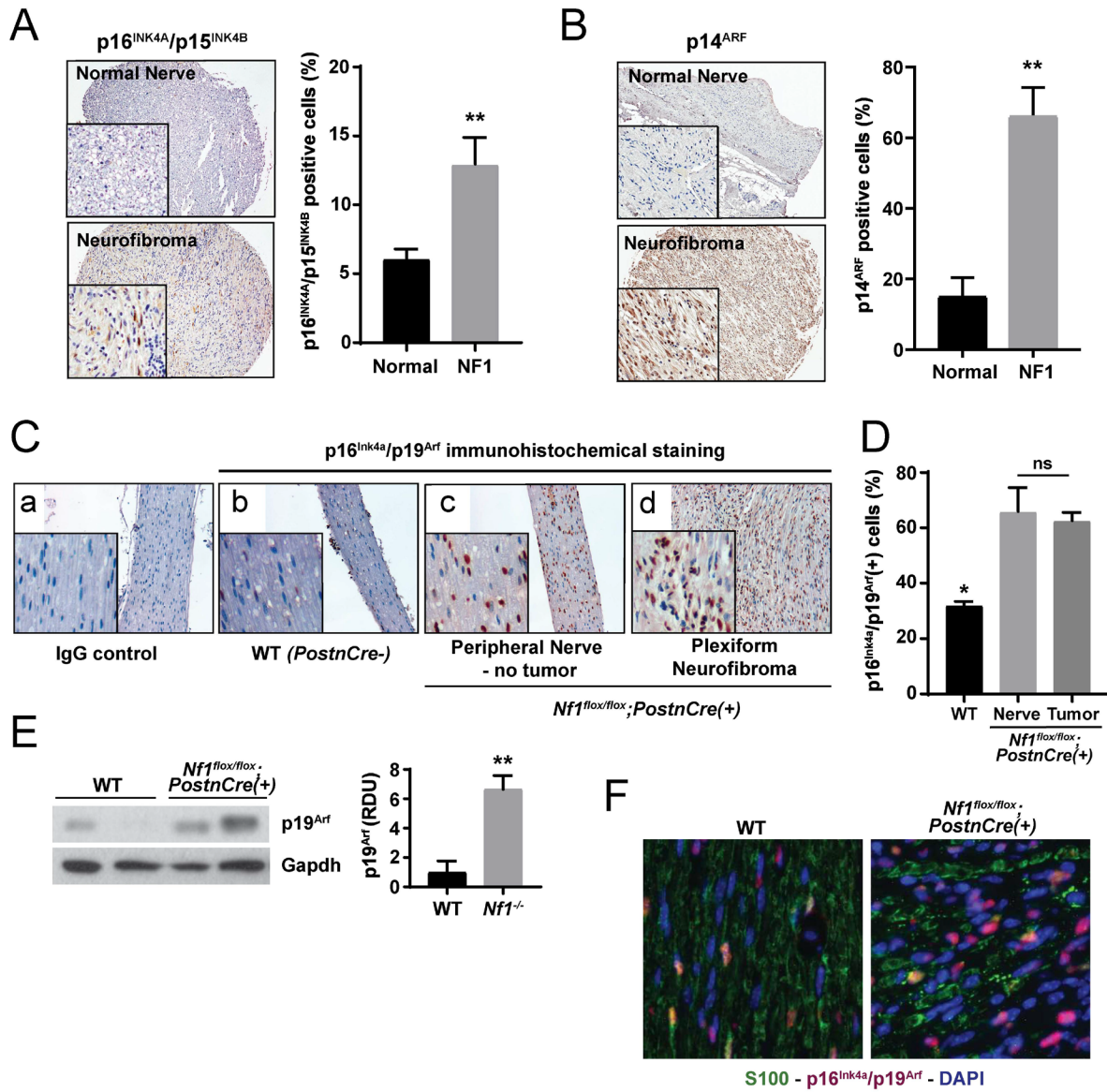
magnification.

A   p16^{INK4A}/p15^{INK4B}

Normal Nerve

Neurofibroma

B   p14^{ARF}

Normal Nerve

Neurofibroma

C   p16^{Ink4a}/p19^{Arf} immunohistochemical staining

a   b   c   d

IgG control   WT *(PostnCre-)*   Peripheral Nerve - no tumor   Plexiform Neurofibroma

Nf1^{flox/flox};PostnCre(+)

D

E   WT   *Nf1^{flox/flox}; PostnCre(+)*

p19^{Arf}

Gapdh

F   WT   *Nf1^{flox/flox}; PostnCre(+)*

S100 - p16^{Ink4a}/p19^{Arf} - DAPI

Figure 2

Figure 3. Genetic ablation of p19^{Arf} allows *Nf1-null* DNSCs to escape senescence and proliferate aberrantly

A. Proliferation of WT, *Nf1$^{-/-}$*, *Nf1$^{-/-}$;Arf$^{+/-}$* and *Nf1$^{-/-}$;Arf$^{-/-}$* DNSCS was assessed by manual cell counting at serial timepoints as shown. The fold change in cell number relative to input (50,000 cells/well) is shown.

B. Cell cycle of WT, *Nf1$^{-/-}$*, *Nf1$^{-/-}$;Arf$^{+/-}$* and *Nf1$^{-/-}$;Arf$^{-/-}$* DNSCS was assessed by flow cytometry. The percentage of cells in G0/G1, S, and G2/M phase are denoted as shown.

C. Senescence associated β-galactosidase staining in DNSCs as shown in representative photomicrographs.

D. The percentage of SAS-βgal-positive staining cells relative to total cell number per HPF was quantified. ****$p<0.0001$ for *Nf1$^{-/-}$* vs WT, *Nf1$^{-/-}$;Arf$^{+/-}$* and *Nf1$^{-/-}$;Arf$^{-/-}$* by one-way ANOVA followed by Tukey's multiple comparison's test. *n*=3 biological replicates per genotype.
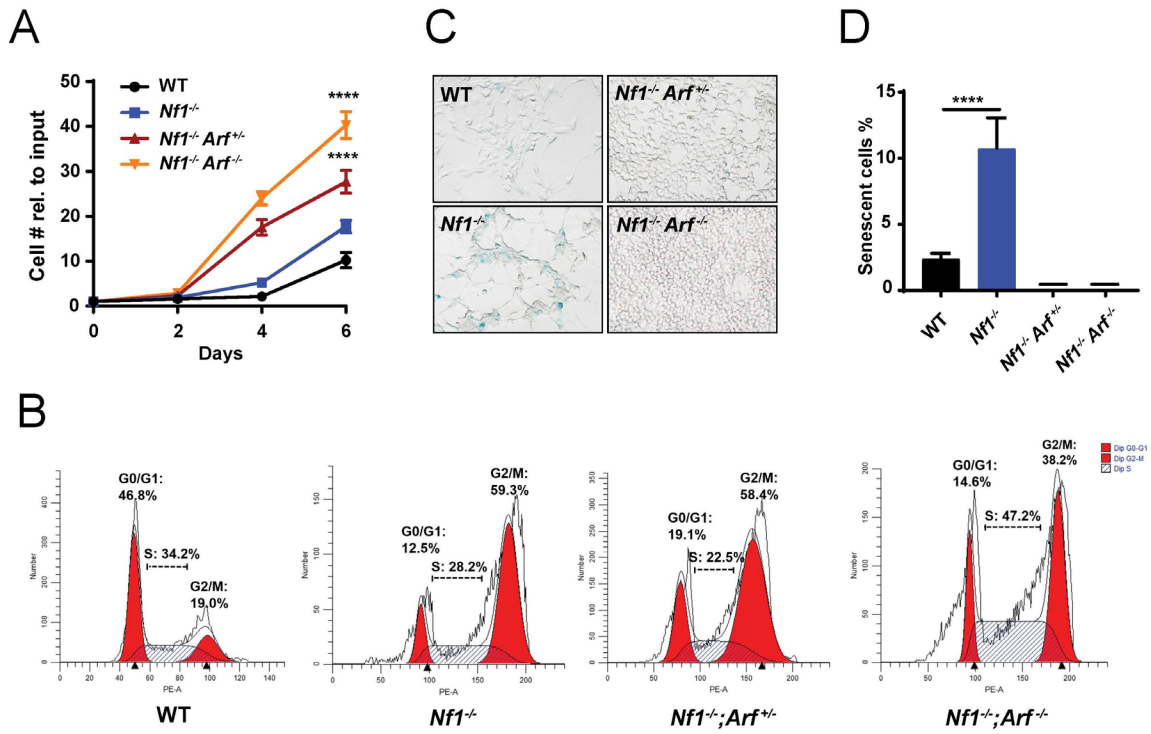
A

B

C

D

Figure 3

Figure 4. **Diffuse morphological changes in the lumbosacral nerve plexus of *Nf1/Arf* mutant mice**

A. The lumbosacral spinal cord, DRG and associated proximal spinal nerve roots were microdissected from each genotype: WT, *Nf1^{flox/flox}*, *Nf1^{flox/flox};Arf^{flox/+}*, and *Nf1^{flox/flox};Arf^{flox/flox};PostnCre(+)* as shown.

B. Proximal spinal nerve root volume was measured. The number of proximal spinal nerve roots evaluated per genotype are as follows: WT (*n=28*), *Nf1^{flox/flox};PostnCre(+)* (*n=16*), *Nf1^{flox/flox};Arf^{flox/+};PostnCre(+)* (*n=16*), and *Nf1^{flox/flox};Arf^{flox/flox};PostnCre(+)* (*n=24*). **p<0.05* WT vs *Nf1^{flox/flox};PostnCre(+)*. ****p<0.001* WT vs *Nf1^{flox/flox};Arf^{flox/+};PostnCre(+)*. *****p<0.0001* WT vs *Nf1^{flox/flox};Arf^{flox/flox};PostnCre(+)*. Statistical analysis was performed via one-way ANOVA followed by Sidak's multiple comparison test.

C. Western blot of $p19^{Arf}$ and Gapdh (loading control) in the trigeminal nerve of each genotype.
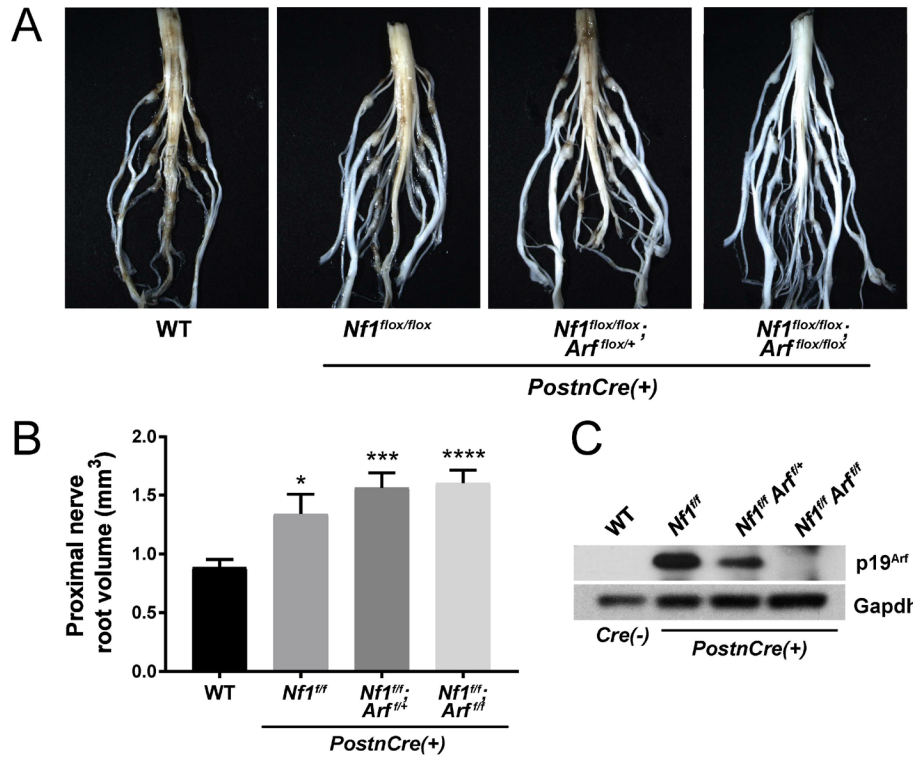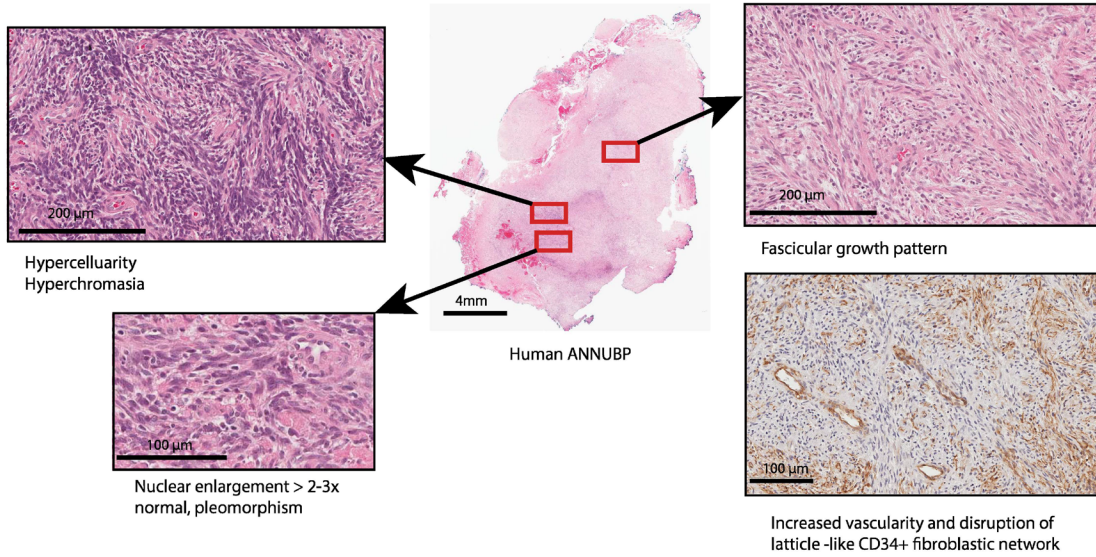
A

WT $Nf1^{flox/flox}$ $Nf1^{flox/flox};$
$Arf^{flox/+};$ $Nf1^{flox/flox};$
$Arf^{flox/flox};$

PostnCre(+)

B

C

Figure 4

Figure 5. *Nf1/Arf* mutant mice develop tumors that phenocopy human ANNUBP.

A. Tumor arising in a 60-year old female patient with a diagnosis of NF1 demonstrating increased cellularity, cytological atypia (enlarged, hyperchromatic and pleomorphic appearing nuclei), fascicular growth pattern and disruption of the lattice like CD34+ fibroblastic network meeting diagnostic criteria ANNUBP.

B. ANNUBP arising in a representative $Nf1^{flox/flox};Arf^{flox/+};PostnCre(+)$ mouse recapitulating the histopathological features observed in the human specimen shown above.

A   Human ANNUBP

Hypercelluarity
Hyperchromasia

Nuclear enlargement > 2-3x
normal, pleomorphism

Human ANNUBP

Fascicular growth pattern

Increased vascularity and disruption of
latticle -like CD34+ fibroblastic network

B   Murine ANNUBP

Hypercelluarity, hyperchromasia
Absent mitoses

Nuclear enlargement > 2-3x
normal, pleomorphism

Core biopsy for next
gen sequencing

Murine ANNUBP
$Nf1^{flox/flox}$;$Arf^{flox/+}$;$PostnCre$ (+)

Fascicular growth pattern

Increased vascularity and disruption of
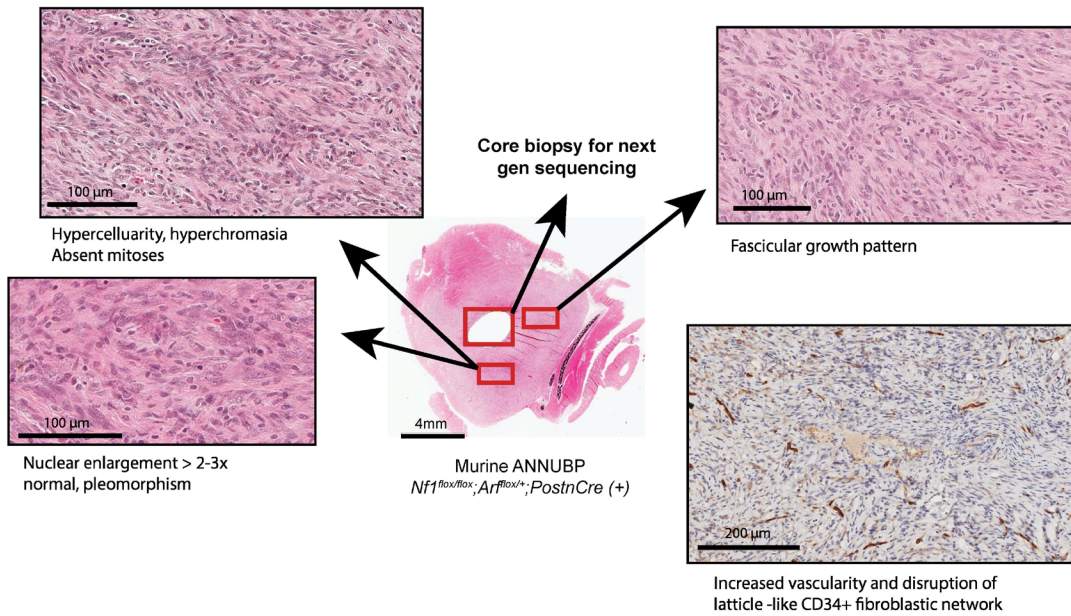latticle -like CD34+ fibroblastic network

Figure 5

Figure 6. **Frequency and size of PN and ANNUBP arising from the cervicothoracic spine of**

***Nf1/Arf* mutant mice.**

A. Coronal whole spinal sections revealing the spinal cord, dorsal root ganlgia (DRG) with

   associated proximal spinal nerve roots demonstrating PN and ANNUBP arising from the

   proximal nerve roots of $Nf1^{flox/flox}$;PostnCre(+), $Nf1^{flox/flox}$;$Arf^{flox/+}$;PostnCre(+) and

   $Nf1^{flox/flox}$;$Arf^{flox/flox}$;PostnCre(+) mice. WT mice exhibited normal nerve architecture and

   cellularity.

B. Stacked bar plot demonstrating the frequency of PN and ANNUBP arising in the cervical

   thoracic spinal nerve roots of $Nf1^{flox/flox}$, $Nf1^{flox/flox}$;$Arf^{flox/+}$ and

   $Nf1^{flox/flox}$;$Arf^{flox/flox}$;PostnCre(+) mice. The number of proximal spinal nerve roots

   evaluated per genotype are as follows: WT (*n*=85), $Nf1^{flox/flox}$;PostnCre(+) (*n*=85),

   $Nf1^{flox/flox}$;$Arf^{flox/+}$;PostnCre(+) (*n*=87), and $Nf1^{flox/flox}$;$Arf^{flox/flox}$;PostnCre(+) (*n*=86).

C. The maximal diameter of WT control nerve roots and those infiltrated with PN and

   ANNUBP lesions were measured on coronal spinal sections and plotted as shown. The

   number of nerve roots and tumors of each histological subtype are as follows: Normal

   nerve (*n*=33), PN (*n*=27) and ANNUBP (*n*=13). Statistical analysis was performed by

   one-way ANOVA followed by Tukey's multiple comparisons test. *$p<0.05$ normal nerve
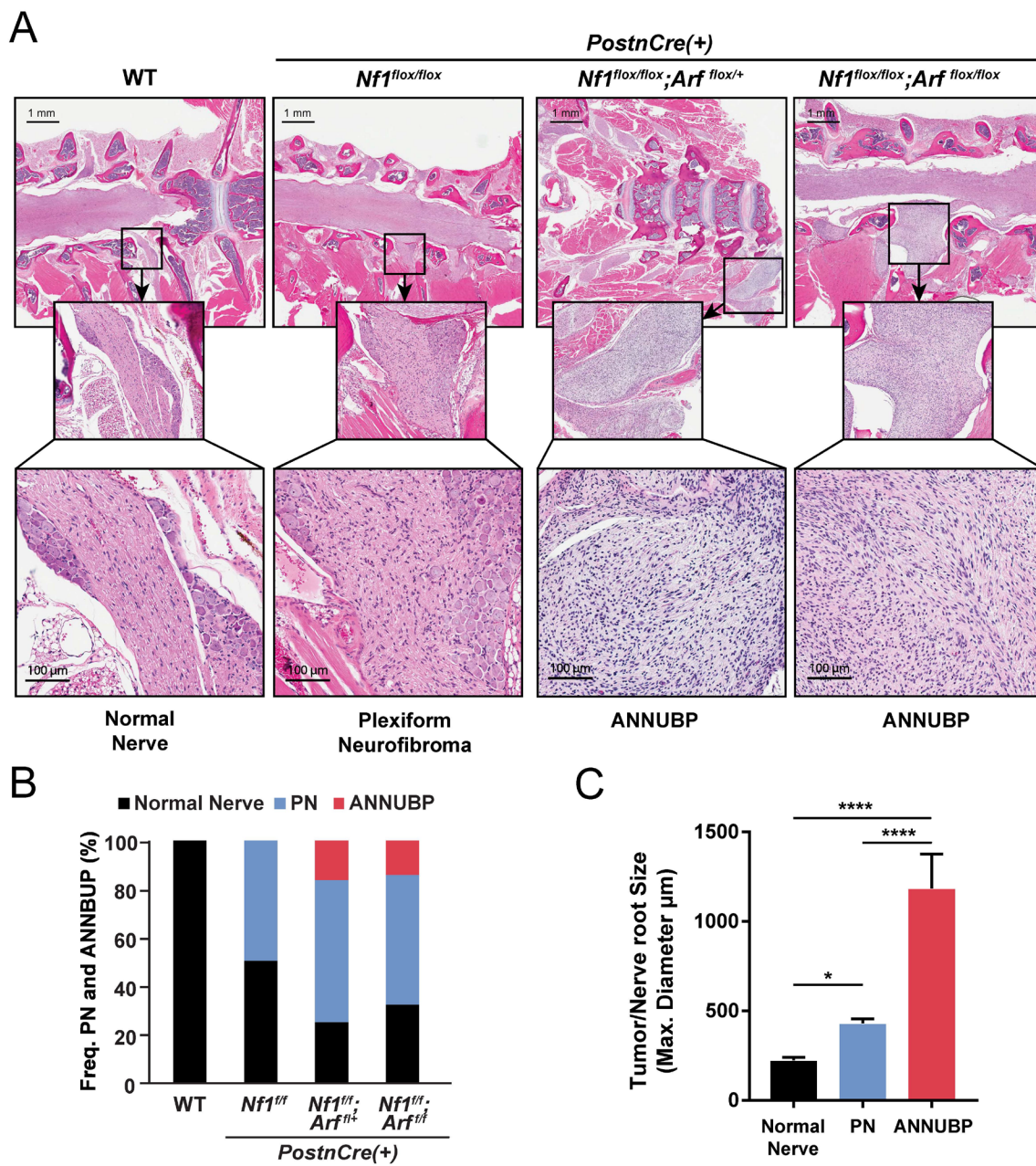
   vs PN. ****$p<0.0001$ ANNUBP vs normal nerve and PN.

Figure 6

Figure 7. *Nf1/Arf* **mutant mice die from tumor progression to MPNST**

A. *Nf1$^{flox/flox}$;Arf$^{flox/flox}$;PostnCre(+)* mouse with multiple, rapidly growing and infiltrative masses. A diagnosis of MPNST was confirmed histopathologically post-mortem.

B. PN arising from a thoracic nerve root in a representative *Nf1$^{flox/flox}$;Arf$^{flox/flox}$;PostnCre(+)* mouse. Progression to ANNUBP is observed with hypercellularity, cellular atypia and a fascicular growth pattern. Subsequent transition to MPNST with encasement/ invasion of surrounding rib and multiple mitotic figures is seen.

C. Kaplan Meier survival curve of WT (*n*=14), *Arf$^{flox/flox}$;PostnCre(+)* (*n*=9) *Nf1$^{flox/flox}$* (*n*=17), *Nf1$^{flox/flox}$;Arf$^{flox/+}$;PostnCre(+)* (*n*=17) and *Nf1$^{flox/flox}$;Arf$^{flox/flox}$;PostnCre(+)* (*n*=16) mice. Statistical analysis was performed using a logrank test with Bonferroni post-hoc adjustment for multiple comparisons. ***p<0.001 *Nf1$^{flox/flox}$;Arf$^{flox/flox}$;PostnCre(+)* vs WT, *Arf$^{flox/flox}$;PostnCre(+)* and *Nf1$^{flox/flox}$;PostnCre(+)*. **p<0.01 *Nf1$^{flox/flox}$;Arf$^{flox/flox}$;PostnCre(+)* vs *Nf1$^{flox/flox}$;Arf$^{flox/+}$;PostnCre(+)*.

A

**Nf1^flox/flox^;Arf^flox/flox^;
PostnCre(+) MPNST**

B

Plexiform neurofibroma

Malignant Peripheral Nerve Sheath Tumor

50 μm

500 μm

25 μm

50 μm

Mitotic Figures

Site of origin:
thoracic nerve

**Nf1^flox/flox^;Arf^flox/flox^;
PostnCre(+)**

ANNUBP

50 μm

4 mm

500 μm

Malignant transformation
Tumor invading/encasing rib

C

Age (months)

Percent survival

- WT
- Arf^f/f^
- Nf1^f/f^
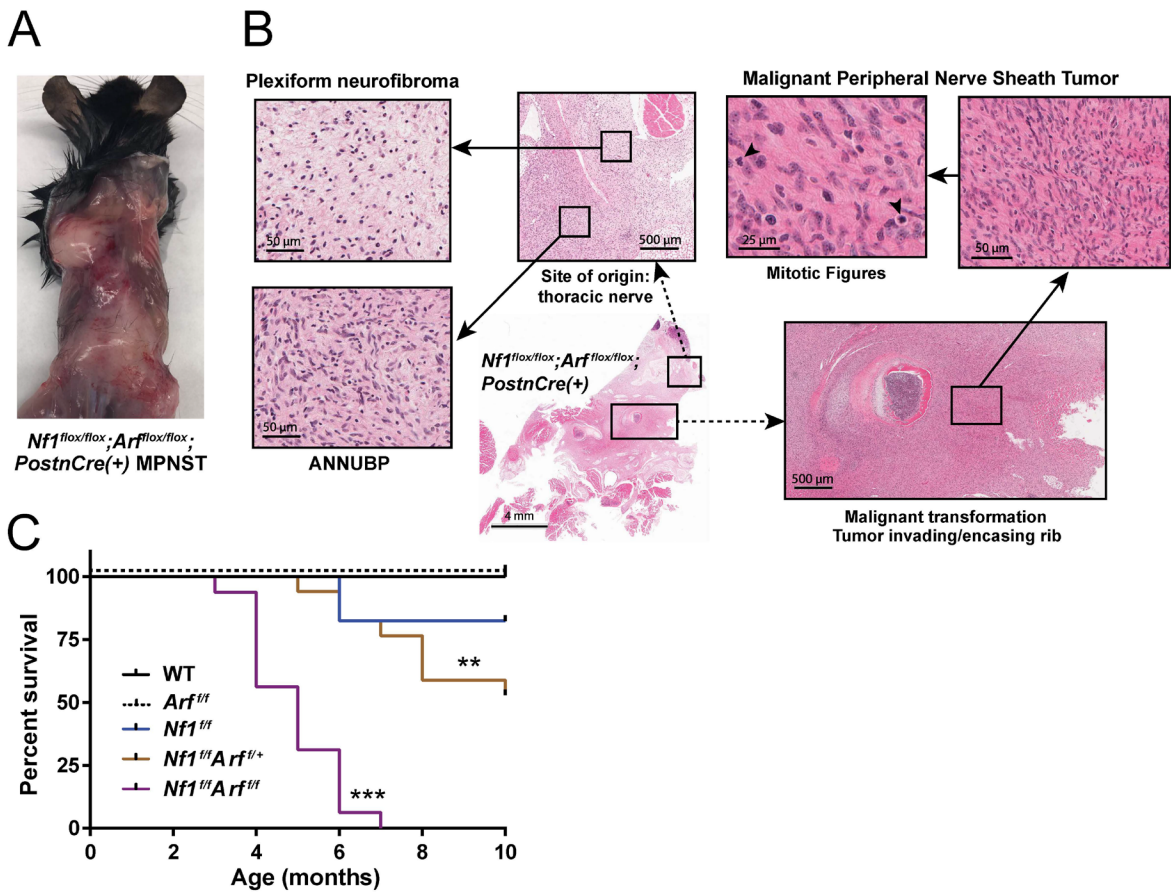- Nf1^f/f^Arf^f/+^
- Nf1^f/f^Arf^f/f^

**

***

Figure 7

Table 1. Histopathological features and diagnostic criteria for NF1-associated peripheral nerve sheath tumors.

Diagnosis	Key Diagnostic Features*
Plexiform Neurofibroma (PN)	Neoplastic proliferation of S100+ Schwann cells with wavy nuclear contours, diffusely enlarging and replacing a major nerve trunk. Thickened perineural sheath. Microenvironment consisting of fibroblasts with myxoid/collagenous matrix and infiltrating inflammatory cells (mast cells and other lineages). Well-developed, lattice like CD34+ fibroblastic network.
Atypical Neurofibromatous Neoplasm of Uncertain Biologic Potential (ANNUBP)	Schwann cell neoplasm with at least 2 of 4 features: (1) Hypercellularity as defined by nuclear overlap at high magnification; (2) Cytologic atypia - enlarged nuclei at least 2-3x > normal, hyperchromasia, pleomorphism with irregular chromatin distribution, and/or multinucleated and "bizarre" forms; (3) Loss of neurofibroma architecture as defined by fascicular growth pattern or disruption of lattice like CD34+ fibroblastic network; (4) Rare mitoses with a mitotic index > 1/50 HPF but < 3/10 HPF.
Malignant Peripheral Nerve Sheath Tumor (MPNST)	Features of ANNUBP with mitotic index of 3-9/10 HPF without necrosis (Low Grade MPNST). MPNST with a mitotic index >10/10 HPF or >3/10 HPF with necrosis (High Grade MPNST).

*Adapted from Miettinen et al. *Human Pathology* (2017) 67, 1-10.

ABREVIATIONS

NF1 – neurofibromatosis type 1

PN – plexiform neurofibroma

ANNUBP – atypical neurofibromatous neoplasm of uncertain biological potential

MPNST – malignant peripheral nerve sheath tumor

PostnCre – PeriostinCre

Arf – Cdkn2a alternate reading frame

SC – Schwann cell

DRG - dorsal root ganglia

DNSCs - dorsal root ganglion (DRG)/nerve root neurosphere cells

GEM - genetically engineered mouse

ANOVA – analysis of variance

SAS-βgal – senescence associated β-galactosidase

IHC – immunohistochemical